ACS APPLIED MATERIALS & INTERFACES

Research Article

Cite This: ACS Appl. Mater. Interfaces XXXX, XXX, XXX-XXX

www.acsami.org

Overcoming Catalyst Residue Inhibition of the Functionalization of Single-Walled Carbon Nanotubes via the Billups–Birch Reduction

Kevin S. Zhang,[†] David Pham,[†] Olawale Lawal,[§] Saunab Ghosh,[†,‡] Varun Shenoy Gangoli,[†,‡] Preston Smalley,[†] Katherine Kennedy,[†] Bruce E. Brinson,[†,‡] W. Edward Billups,[‡] Robert H. Hauge,[‡] W. Wade Adams,[*,§] and Andrew R. Barron[β*,‡,∥]

[†]Smalley-Curl nanoCarbon Center, Rice University, Houston, Texas 77005, United States

[‡]Department of Chemistry, Rice University, Houston, Texas 77005, United States

[§]Department of Materials Science and Nanoengineering, Rice University, Houston, Texas 77005, United States

[∥]Energy Safety Research Institute (ESRI), Swansea University Bay Campus, Fabian Way, Swansea SA1 8EN, U.K.

Supporting Information

ABSTRACT: The Billups–Birch Reduction chemistry has been shown to functionalize single-walled carbon nanotubes (SWCNTs) without damaging the sidewalls, but has challenges in scalability. Currently published work uses a large mole ratio of Li to carbon atoms in the SWCNT (Li:C) to account for lithium amide formation, however this increases the cost and hazard of the reaction. We report here the systematic understanding of the effect of various parameters on the extent of functionalization using resonant Raman spectroscopy. Addition of 1-iodododecane yielded alkyl-functionalized SWCNTs, which were isolated by solvent extraction and evaporation, and purified by a hydrocarbon wash. The presence of SWCNT growth catalyst residue (Fe) was shown to have a strong adverse effect on SWCNT functionalization. Chlorination-based SWCNT purification reduced the amount of residual Fe, and achieve a maximum I_D/I_G ratio using a Li:C ratio of 6:1 in a reaction time of 30 min. This result is consistent with published literature requiring 20-fold mole equivalents of Li per mole SWCNT with a reaction time of over 12 h. This new understanding of the factors influencing the functionalization chemistry will help cut down material and process costs, and also increase the selectivity of the reaction toward the desired product.

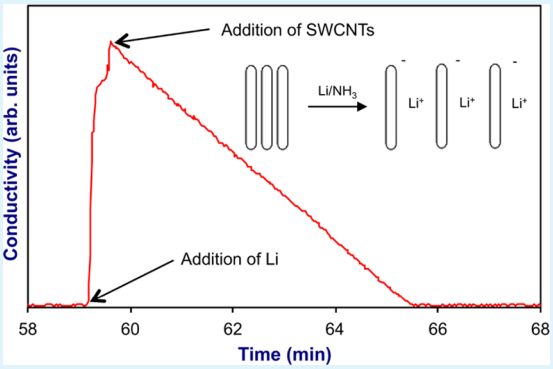

KEYWORDS: *carbon nanotube, lithium, ammonia, Billups–Birch reduction, iron oxide*

INTRODUCTION

The ability to covalently functionalize single-walled carbon nanotubes (SWCNTs) overcomes both their bundling and lack of solubility/miscibility. A wide range of methods have been reported and each has advantages and disadvantages.[1−5] A convenient one-pot approach to covalent sidewall functionalization of SWCNTs uses the Li metal/liquid ammonia-based chemistry via the Billups–Birch reduction (Scheme 1).[6−8] An analogous reaction with Na/Hg amalgam results in similar products, albeit with a lower number of alkyl groups per carbon atom in the SWCNT.[9] The resultant alkyl functionalized SWCNTs (R-SWCNTs) are highly soluble in solvents such as chloroform, THF and water. The importance of this process is clear when coupled with the report that the thermal defunctionalization of R-SWCNTs is selective with respect to the nanotube diameter, offering a scalable route to SWCNT separation of chirality and/or electronic properties.[10]

In traditional solutions formed by dissolution of a Group 1 metal in liquid NH_3, the electron is stabilized within an ammonia cluster solvation.[11,12] In the presence of SWCNTs the formation of a polyanionic nanotube, $[SWCNT]^{n-}$, provides the stabilization. It is this polyanion that reacts with an alkyl halide to yield an alkyl-functionalized SWCNT.[13] In the case of

Scheme 1. Schematic Representation of the Alkyl Functionalization of SWCNTs via the Billups–Birch Reduction Using Li/NH_3 with Subsequent Reaction with an Alkyliodide, e.g., 1-Iodododecane

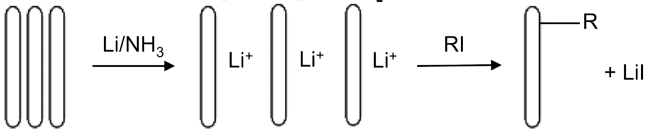

Received: August 25, 2017
Accepted: October 12, 2017

DOI: 10.1021/acsami.7b12857
ACS Appl. Mater. Interfaces XXXX, XXX, XXX−XXX

sodium/THF reduction the polyanion can be stabilized by the addition of dibenzo-18-crown-6.[9]

The original Billups–Birch reaction process was performed in a three-necked flask/Dewar condenser setup for 24 h with the flask submerged in an acetone-dry ice mixture and uses a 19-fold excess of Li.[6−8] This simple setup has several limitations, however, since no information on the extent or rate of reaction is provided. The scalable synthesis of highly solubilized undamaged nanotubes requires a more robust and controllable approach. We have recently reported an in-house developed dual-reactor apparatus[14] to functionalize SWCNTS in a highly reproducible and scalable (300−500 mg, equivalent to 25−42 mmol based on 1 mol SWCNT = 12 g as per reported literature[6]) manner. Furthermore, the ability to in situ monitor the conductivity of the reaction solution was included to determine the extent and rate of the reduction and alkylation reactions.[14] One important result of this prior work was that a typical dodecylation reaction of SWCNTs is completed much earlier (30 min instead of 24 h) and requires less metallic lithium than previously reported.[6−8,14] However, during this study we noted that there was an instability in the Li/NH_3/SWCNT solution that depended on the sample/batch of SWCNTs being used. This was found to complicate the use of the process for the purification, and separation of SWCNTs,[10,15] and thus merited a deeper study.

Feng et al. have reported that ammonia adsorption onto the surface of SWCNTs is sensitive to the functional groups and defects on the nanotube surfaces,[16] suggesting that the purity of the SWCNTs may influence the stability of the reduced species. Recently, we have shown that the presence of residual catalyst (iron oxide in the case of HiPco SWCNTs[17]) results in the oxidation of zerovalent Group 6 metal species.[18] A similar reaction is possible in the case of the Li/NH_3 system. Residual catalyst has also been of concern in the application of CNTs for biological systems.[19,20]

In order to determine the optimum conditions for large scale SWCNT functionalization, it is important to understand the limitations of the process and optimize based on real-time monitoring of the reaction. We have therefore investigated the reduction and alkylation process through in situ monitoring using the conductivity of the reaction solution, as well as sample extraction and ex-situ characterization of the products. The results of this study are reported herein.

EXPERIMENTAL SECTION

Materials and Reagents. Pristine HiPco single-walled carbon nanotubes (SWCNTs), 09-HiPco-0093 batch number 190.1, were obtained from the Carbon Nanotube Laboratory (CNL) at Rice University and used as received unless stated otherwise. Graphite (99.99% powder, synthetic, < 45 μm), Lithium (granule, high sodium, 99%), tetrahydrofuran (≥99.9%), hexane (≥98.5%), 1-iodododecane (98%), acetone, ethanol (200 proof), and Millipore PTFE (0.2 μm) filter paper were obtained from Sigma-Aldrich and used as received unless otherwise noted.

Characterization. All characterization for the samples were performed either prior to or after the reaction process was completed. Thermogravimetric analysis (TGA) was conducted on a TA Instrument SDT Q600. The samples were run in an open alumina crucible under continuous air flow of 100 mL·min^{-1} with a heating ramp rate of 10 °C·min^{-1}. Raman spectra were collected in a Renishaw Raman microscope equipped with a 633 nm excitation laser, with the SWCNT samples as either powder or Buckypaper placed on a microscope glass slide. X-ray photoelectron spectra (XPS) were recorded on a PHI Quantera XPS Scanning Microprobe using a monochromated Al–K_α source. All spectra were recorded using a charge neutralizer to limit differential charging and subsequently calibrated to the carbon peak at a binding energy of 284.5 eV. Survey scans were recorded at a pass energy of 140 eV and high-resolution data at a pass energy of 26 eV. Before spectral fitting, each spectrum was corrected for reference binding energy for C 1s to 284.5 eV. The data were fitted using MultiPak software.

Chlorine Purification of SWCNTs. Chlorine treatment was completed using a modification of a process previously reported.[21] The SWCNT sample was compacted into a graphite casing, which was inserted into a quartz tube. The sample was heated to 600 °C under a low vacuum (−30 psi), after which Ar (200 mL·min^{-1}) was passed through the system to assist in the removal of desorbed species. Cl_2 gas was slowly introduced into the system until system pressure reached 15 psi. The sample was soaked in a chlorine atmosphere for 30 min, after which a diaphragm pump was used to purge the system. Repeated, vacuum/Ar/Cl_2 cycles were used as required. After the final purge, the furnace was cooled to room temperature (25 °C) and the sample removed. Microwave pretreatment was also examined to help remove the amorphous carbon allowing encapsulated iron to be removed with the chlorine purification process,[22] using an 800 W microwave for 10 × 1 min cycles, after which a 3-cycle chlorine purification process was administered. The different purification protocols are described in Table 1.

Table 1. Summary of Various Chlorine and Microwave Purification Treatments

sample	Cl_2 treatment (x 15 min)	microwave (mins)
SWCNT	0	
SWCNT-1Cl	1	
SWCNT-2Cl	2	
SWCNT-3Cl	3	
SWCNT-4Cl	4	
SWCNT-MW-3Cl	3	10

Lithium Reduction and Alkylation of SWCNTs. The reactions were performed in the Hauge twin reactor apparatus described previously.[14] In a typical reaction, SWCNTs (4.2 mmol) were added to the reaction flask and heated under vacuum at 180 °C for 10 min in order to remove adsorbed gases. The flask was then submerged in a dry ice-acetone bath (−78 °C) to condense NH_3 (ca. 300 mL). Li metal was weighed in a mass balance placed in a sealed glovebag under argon, and taken out in an airtight container. The desired amount of Li metal was added to the reactor via the insertion chamber as described previously[14] in molar quantities (C:Li = 1:1−6) until a conductive solution was created as measured by the LabQuest Pro conductivity probe. Shear-mixing homogenization ensures homogeneity of the solution. The conductivity was measured as a function of time. Additional quantities of Li metal were added as described in the Results and Discussion section

Lithium Reduction of Graphene. Functionalization proceeded according to the method employed for SWCNTs, but with graphene (37.5 mmol). In addition, once a stable conductivity was observed, the reaction mixture was allowed to rise to room temperature. The reactivity of the Li/NH_3/graphene solution was tested by exposure to the atmosphere.

Alkylation of SWCNTs. Functionalization proceeded according to methods described by Billups' alkylation of nanotubes using Birch reduction.[6,13,14] To a sample of Li/NH_3/SWCNT (see above) was added a solution of 1-iodododecane (2 mL) in THF (3 mL). The solution was stirred for 2 h, after which the liquid NH_3 was extracted to the sample collector to prevent contamination of the functionalized product from any side products formed during reaction. C_{12}–SWCNTs were extracted into a separatory funnel, to which EtOH (150 mL), DI water (150 mL), and hexane (200 mL) was added sequentially. A solution of diluted HCl (10 mL) was added to the funnel and the solution was vigorously shaken. The hexane layer was filtered through a cellulose filter paper after separation from the water/

DOI: 10.1021/acsami.7b12857
ACS Appl. Mater. Interfaces XXXX, XXX, XXX−XXX

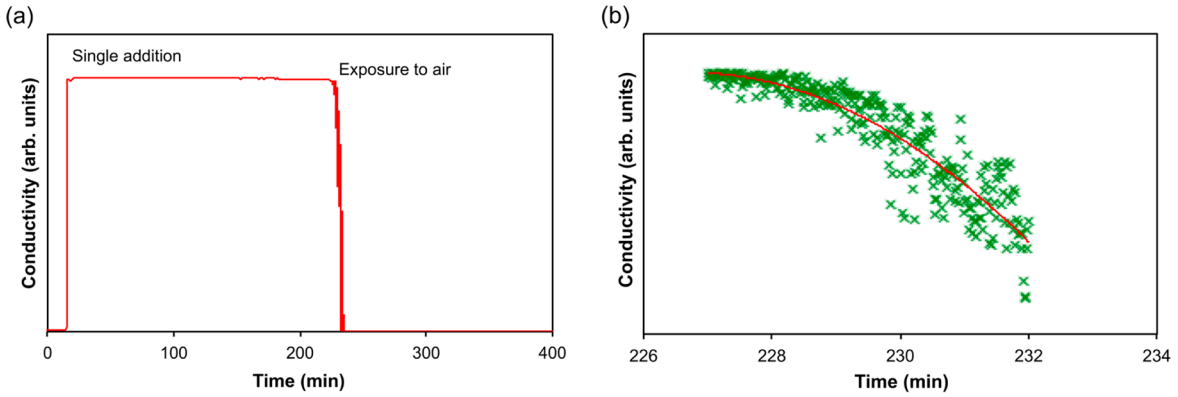

Figure 1. Conductivity plot as a function of time showing (a) the stability until exposure to air of the Li/NH_3 solution at −35 °C and (b) an expansion of the region after exposure to air.

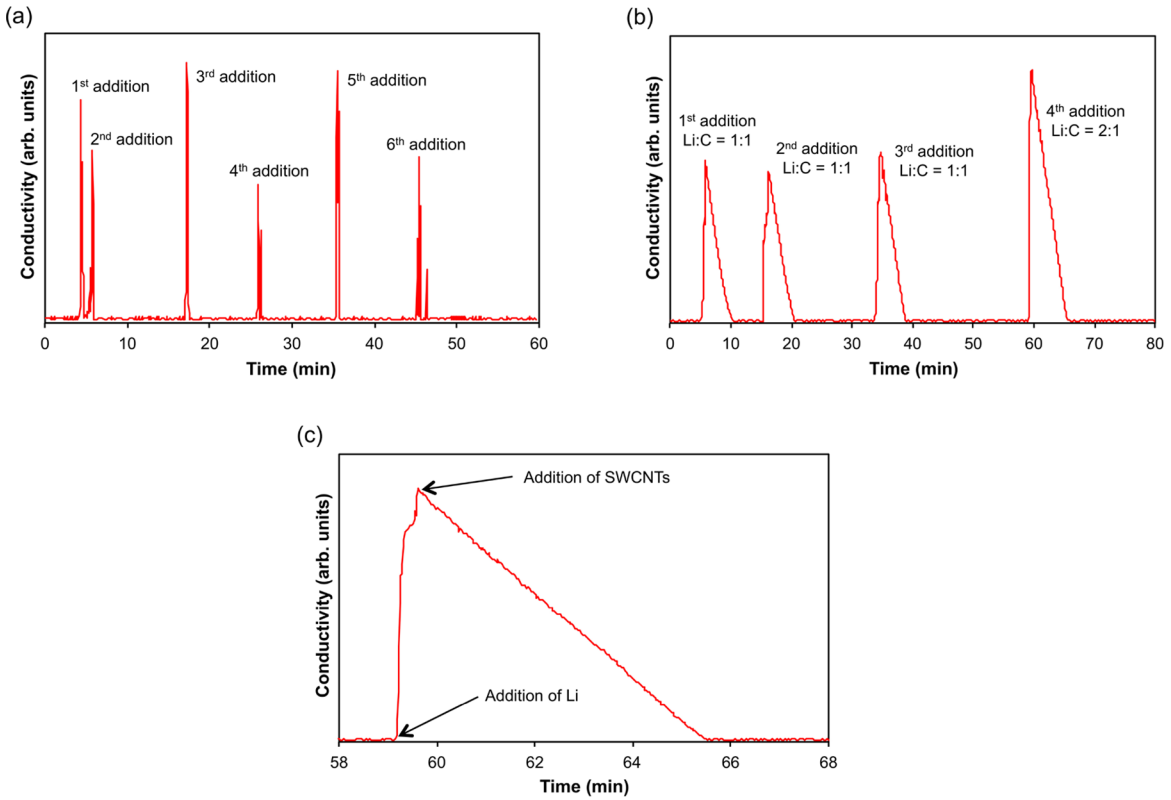

Figure 2. Conductivity plot as a function of time showing (a) the immediate quenching of conductivity upon addition of six additions of excess Li (ca. 12.5 mmol per addition) to an NH_3 solution of raw-HiPco SWCNTs (8.33 mmol) at −35 °C, (b) the quenching of conductivity as a function of time upon addition of 4 additions of excess Li (ca. 21.4 mmol per addition) to an NH_3 solution of raw-HiPco SWCNTs (8.33 mmol) at −75 °C, and (c) an expansion of the quenching after the 4th addition showing the zero-order reaction.

EtOH layer. Products were vacuum-dried overnight and stored as Buckypaper.

RESULTS AND DISCUSSION

Conductivity Tracking of Raw SWCNTs. Liquid NH_3 dissolves lithium metal, forming a blue-colored solution, which is a strong reducing agent containing solvated electrons.[11,12] The addition of Li metal to liquid NH_3 (at −35 °C) results in the formation of a conductive solution that is stable for at least 4 h. Exposure to air results in the immediate quenching of the $Li^+[e^-(NH_3)_n]$ solvate (Figure 1a). This indicates that there is no ingress of oxygen (air) to the reaction chamber, which is confirmed by pressure testing the chamber.[14] Observation of the rate of change of conductivity as a function of time upon exposure to air shows an increase in rate as a function of time (Figure 1b), which is consistent with an exothermic reaction.

Addition of SWCNTs to the strongly reducing Li/NH_3 solution should result in a conductive solution containing $[Li^+]_n[SWCNT]^{n-}$ species; however, whereas in the presence of raw HiPco SWCNTs the addition of Li to liquid NH_3 (at −35 °C) does result in an immediate increase in conductivity, it is then rapidly quenched in less than 1 min (Figure 2a). Addition of further batches of Li result in a subsequent increase in conductivity that is also rapidly quenched. As seen in Figure 2a, the quenching appears to be independent of the time between additions.

DOI: 10.1021/acsami.7b12857
ACS Appl. Mater. Interfaces XXXX, XXX, XXX−XXX

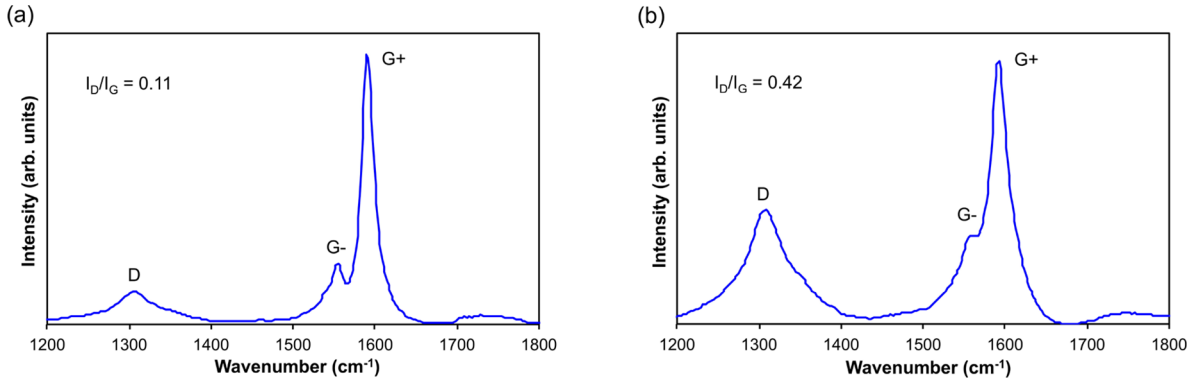

Figure 3. Raman spectra of HiPco SWCNTs after reaction with Li/NH_3 and 1-iodododecane at (a) −35 °C and (b) −75 °C. Due to the curvature of SWCNTs, in contrast to the perfect honeycomb lattice of graphite, the G band splits into the G+ and G- bands.

Completing the functionalization process with these poorly conductive SWCNT samples with an excess of 1-iodododecane resulted in a product that showed Raman spectra (Figure 3a) that is only slightly increased as compared to that of the starting SWCNTs reported in our previous publication using the same raw materials and processes (I_D/I_G = 0.04).[14] The similarity in the I_D/I_G ratio indicates that the degree of alkylation is exceptionally low. We note that the I_D/I_G ratio cannot always be used as a quantitative measure of the degree of functionalization, because the distribution of substituents is also a factor;[23] however, where the identity of the functional group and the synthetic route are identical then valid comparisons may be made. Nevertheless, the Raman data suggest that either the SWCNTs are not receiving free electrons (due to rapid oxidation of the solvated electron species) or any reduced $[SWCNT]^{n-}$ species formed is highly unstable and is being quenched. In addition, the presence of a residual side product of the functionalization process is found after the evaporation of liquid ammonia. We also note that the radial breathing mode (RBM) of the SWCNTs get suppressed postfunctionalization relative to before, as seen in Figure 4, which matches previously reported results.[6] FTIR analysis of the white residual side product confirms[6] the presence of lithium amide ($LiNH_2$), a known oxidation product of the Li/NH_3 solution.

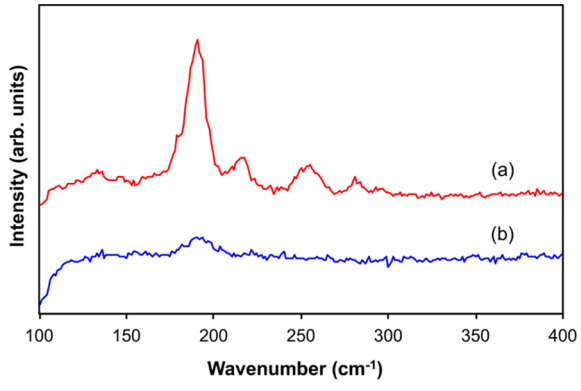

Figure 4. Radial breathing mode (RBM) region of the resonant Raman spectra for the (a) SWCNTs before and (b) after reaction with Li/NH_3 and 1-iodododecane at −35 °C. The spectral intensities have been normalized to the G-peak (not within this range) for ease of comparison.

At this point, the importance of homogeneous mixing in the reaction vessel must be stressed. We noticed during initial experiments that the Raman spectra for the same product sample taken at various points along the sample were significantly different when it came to the I_D/I_G ratio (Figure 5). We collected a total of 12 different spectra, measured I_D/I_G for each, and then plotted the values to note a distribution curve as seen below. In order to determine the average I_D/I_G for the entire sample (0.963), a similar procedure was followed using thermogravimetric analysis as described in an earlier work.[10] We note that this average value (0.955) ends up being very close to the mean value of the individual I_D/I_G from the collected spectra. Allowing the homogenizer to run for 15−20 min before the reaction commences also greatly helps reduce such variation in the extent of functionalization. All experimental runs, and results thereof, were subsequently performed with the effect of mixing accounted for.

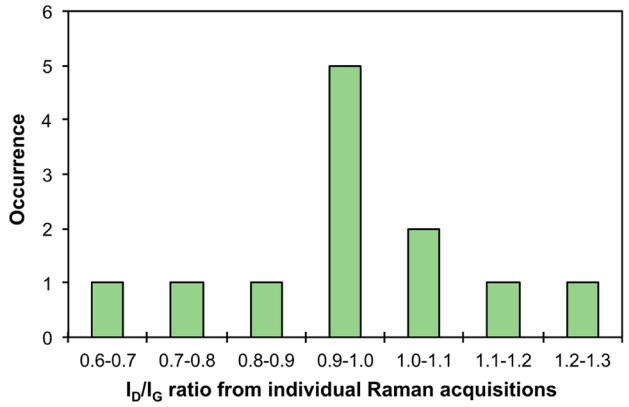

Figure 5. Distribution of I_D/I_G collected for the same sample at various physical points showing a strong effect on the homogeneity of the extent of functionalization of the SWCNTs if not mixed sufficiently.

By analogy with the temperature dependence of the Birch reaction,[24] we theorize that lower temperatures could drive a larger difference between the rates of the primary covalent sidewall functionalization reaction and the lithium amide formation side reaction. Initial Birch reduction of HiPco SWCNTs occurred at −35 °C, near boiling point of ammonia. Theorizing that the rate of covalent functionalization occurs faster than lithium amide formation, functionalization was performed at −75 °C to determine if there is any increase in

DOI: 10.1021/acsami.7b12857
ACS Appl. Mater. Interfaces XXXX, XXX, XXX−XXX

extent of functionalization. As seen in Figure 2b, the conductivity trends display a reduction in quench rate. Although quenching is still observed, the rate is significantly slower (c.f. Figure 2a). After functionalization of the solution with an excess of 1-iododododecane, the Raman spectrum of the resulting product shows an increase in functionalization (Figure 3b) with a D:G ratio of 0.42, consistent with the formation of dodecyl-functionalized SWCNTs (C_{12}−SWCNTs). Relative to initial reaction at −35 °C, this serves as a 5-fold increase in functionalization when considering D:G ratio of 1:1 or higher is indicative of successful covalent functionalization of HiPco SWCNTs using a dodecyl halide functional group.[13,14]

As noted in the Introduction, the presence of residual oxidized iron catalyst in HiPco SWCNTs resulted in the oxidation of $M(CO)_6$ (Cr, W) to the oxide.[18] Given the redox potential of Fe^{3+}, it is possible a similar process is occurring between the catalyst residue and the solvated electrons or $[SWCNT]^{n-}$ species. In order to test this, raw HiPco SWCNTs were mixed with different C:Li ratios and after reaction the quenched samples were analyzed by high resolution Fe 2p XPS in order to determine the relative Fe(O):Fe(II):Fe(III) ratios (SI Figure S1).[18] As may be seen from Table 2, while some

Table 2. XPS Fe 2p Assignment and Relative Composition for Raw SWCNTs and Li/NH_3 Treated SWCNTs

peak (eV)	assignment	raw-HiPco (%)	Li/NH_3 treated (C:Li = 1:5) (%)	Li/NH_3 treated C:Li = 1:20) (%)
707.5	Fe(0)	48.00	46.96	45.85
709.8	Fe(II)	13.13	11.98	9.10
711.4	Fe(III)	38.67	41.07	45.05

variation is observed (as expected from the surface specific nature of XPS) there is no trend consistent with the reduction of Fe(III) or Fe(II) as observed previously.[18] This would suggest that if the catalyst residue is responsible for the quenching of the reduced SWCNT species, it is catalytic rather than stoichiometric.

Closer inspection of the quenching observed in the conductivity measurements (Figure 2a and b) reveals that unlike the air quenching of Li/NH_3 (Figure 1b), the reactions are zero-order, for example, Figure 2c. Zero-order kinetics is consistent with catalytic reactions where the catalyst surface is saturated with reagent. Given that the "solubilized" SWCNTs and/or the catalyst residue associated with each tube would be solvated with NH_3, then the observed kinetics would be consistent with either the SWCNT or the catalyst residue, catalyzing the quenching of the reduced species. Analysis of the data in Figure 2a and b using the Arrhenius equation shows a rate constant (k) of the quenching to be 190 ± 30 s^{-1} and 10.4 ± 0.7 s^{-1} for the reaction at −35 °C and −75 °C, respectively. Consequently, an E_a for the quenching reaction may be calculated (28 ± 2 kJ mol^{-1}).

If the iron catalyst residue catalyzes the quenching, then the Fenton oxidation could be a comparable reaction, whereby Fe(II) and Fe(III) undergo electron transfer. The kinetics of the Fenton reaction have been extensively studied and the activation energy is ordinarily in the range of 2−50 kJ mol^{-1}.[25−28] Our determined value is clearly within this rather broad range, suggesting that it is consistent with (although not unique to) a comparable electron transfer reaction.

Conductivity Tracking of Graphene. To confirm the effect of catalyst residue, the conductivity of liquid NH_3 with graphene was investigated. In contrast to SWCNTs, graphene can be prepared with high purity (99.9999%), and the lack of catalyst residue should preclude the undesired quenching reaction. However, if it is the presence of oxygen functional groups that are causing the quenching,[16] then the epoxide functionality on the graphene should also cause quenching.[29] Lithium-intercalated graphene has previously been reported by the Billups−Birch reduction using an excess of Li.[30]

A conductivity plot of graphene in lithiated liquid NH_3 in inert atmosphere is shown in Figure 6. The conductivity is

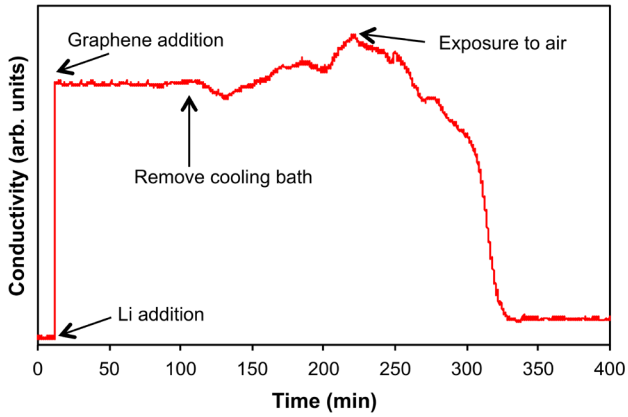

Figure 6. Conductivity plot of graphene/NH_3 upon addition of Li metal, and after removal of the cooling bath and exposure to air.

stable and shows no quenching. After 2 h at −78 °C, the reaction was allowed to warm by the removal of the dry ice-acetone bath. During this time the NH_3 remained liquid (i.e., the temperature stayed below −33 °C). As expected, the conductivity increased with increasing temperature, which matches published results.[31] After a further 2 h, the sample was exposed to air, resulting in a decline in the conductivity consistent with oxidation of the reduced $[graphene]^{n-}$ species. This result is also consistent with the catalyst residue in the HiPco SWCNTs causing the oxidation of the SWCNTs, and suggests that improved purification should enhance the stability of the reduced SWCNT species, and hence the efficiency of functionalization.

Purification Process to Remove Metal Impurities. From the forgoing it is probable that the residual iron oxide catalyst residue is responsible for the quenching of the reduced SWCNT species and the low extent of functionalization. We postulate that to improve functionalization it is necessary to remove as much of the catalyst residue as possible. Chemical purification methods commonly use gas-phase[32−34] and wet-chemistry methods.[33−36] While liquid-phase oxidation is effective in removing both amorphous carbon and metallic catalyst particles, it generally requires the use of strong oxidants.[37−39] These oxidation routes result in the sidewall of the SWCNT becoming functionalized with oxygen-containing groups in addition to cutting the SWCNTs.[40] Given that an advantage of the Billups−Birch reduction process is that it does not cut the SWCNTs, it is important to employ a purification process that also limits damage. In addition, adding impurities will further complicate results.

We have recently shown that gas phase chlorination of SWCNTs at high temperatures retains the pristine nature of the SWCNTs while attacking the residual iron catalyst at high temperatures to form volatile $FeCl_3$ that is removed under

DOI: 10.1021/acsami.7b12857
ACS Appl. Mater. Interfaces XXXX, XXX, XXX−XXX

vacuum.[21] However, in any sample of raw-HiPco SWCNTs, there are two categories of catalyst residue: exposed and encapsulated. While chlorination appears to remove the former, it is unable to eliminate the catalytic particles that remain encased by either graphitic or amorphous carbon. We have reported that under microwave treatment in air, the carbon shells that encase the residual metal catalyst particles are removed and the metallic iron is exposed and subsequently oxidized making it accessible for chemical removal by chlorination.[22] In order to test this, the Billups–Birch reduction and alkylation was performed on samples of SWCNTs that had been treated with consecutive chlorine treatments, that is, SWCNT-Cl_n, where n = 1–4 (Table 1).

Thermogravimetric analysis (TGA) of raw HiPco SWCNT samples shows about 30 wt % of catalyst residue based on our previous work reported using the same raw sample.[14] In contrast, TGA of SWCNT-1Cl shows decrease in catalyst residue (22 wt %). If, as proposed above, the residue is primarily responsible for oxidation of the reduced SWCNT species, the chlorination should result in an improved functionalization. Raman of subsequent C_{12}–SWCNT shows a dramatic increase in the I_D/I_G ratio = 0.25 (SI Figure S2) over that of the same species formed from raw-HiPco SWCNTs. However, this still does not reach the desired level of functionalization (indicated by a I_D/I_G ratio approaching unity). Upon additional 15 min chlorination cycle (SWCNT-2Cl) the catalyst residue is further reduced and the I_D/I_G ratio of the resulting C_{12}–SWCNT sample shows further improvement. Yet more gains are made by a third chlorination cycle; however, the fourth cycle gave no further improvement (Figure 7). It is interesting to note that the reaction of Cl_2 with the

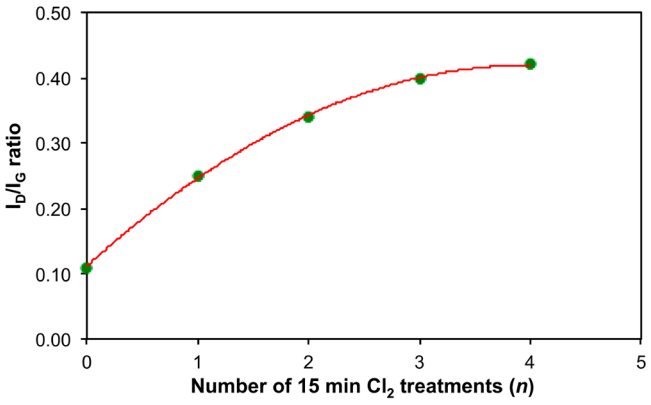

Figure 7. Plot of I_D/I_G ratio obtained from the Raman spectra of the product from the reaction of SWCNT-nCl (where n = number of 15 min treatments) with Li/NH_3 and 1-iodododecane at −35 °C.

catalyst residue ($Fe^0/Fe_3O_4/Fe_2O_3$) at 600 °C is slower than previously assumed.[21] XPS showed minimal presence of chlorine (Table 3). The Cl 2p spectra appears as a broad peak centered at 200 eV, which has been previously characterized[41] as a mixture of chloride associated with iron,[42] atomic chlorine adsorbed on the surface,[43] and chlorine atoms covalently bonded to sp^2 carbon[44−46] in an analogous manner to fluorinated species.[47] Additionally, aspect ratio analysis showed the preservation of nanotube length after chlorine treatment, an issue present in other methods of iron catalyst removal.

Of the possible products from the chlorination of the catalyst residue ($FeCl_3$, $FeCl_2$, and Fe_2Cl_6), the most favored thermodynamically is $FeCl_3$. Three possible reactions between the catalyst residue and Cl_2 occur (eq 1–3), of which that with Fe_2O_3 is endothermic. The kinetics of the reaction of Fe_2O_3 with Cl_2 indicated[48] that diffusion of Cl_2 through the oxide was the rate limiting step. The presence of significant Fe after repeated chlorination suggests that it remains encapsulated (by amorphous carbon diffusion barrier) and is not susceptible to the gas phase reaction. However, the lower than optimum I_D/I_G ratio suggests that the quenching of the reduced SWCNT species can occur even with encapsulated iron oxide residue. To overcome this issue, we have employed a combination of microwave treatment and three cycles of chlorination (SWCNT-MW-3Cl), see experimental.

$$2Fe + 3Cl_2 \rightarrow 2FeCl_3(-399kJ\cdot mol^{-1}) \quad (1)$$

$$2Fe_3O_4 + 9Cl_2 \rightarrow 6FeCl_3 + 4O_2(-160kJ\cdot mol^{-1}) \quad (2)$$

$$2Fe_2O_3 + 6Cl_2 \rightarrow 4FeCl_3 + 3O_2(50kJ\cdot mol^{-1}) \quad (3)$$

Microwave irradiation (800 MW) for 10 × 1 min followed by chlorine treatment (SWCNT-MW-3Cl) resulted in reduction of residual catalyst from 21% to around 5% as determined by TGA (SI Figure S3). Exposure of SWCNT-MW-3Cl to Li/NH_3 shows excellent stability (Figure 8). There appear to be

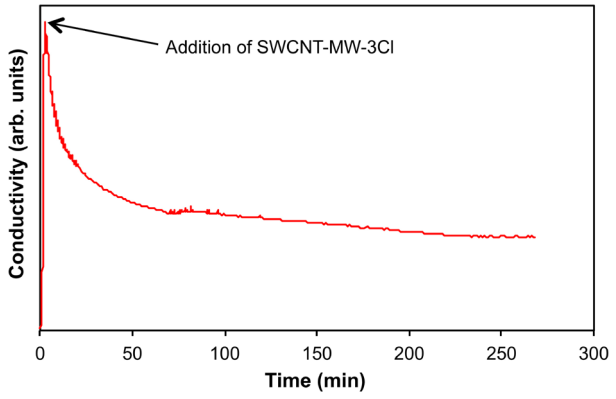

Figure 8. Conductivity plot showing the quenching of conductivity as a function of time upon addition of Li (ca. 12.5 mmol) to an NH_3 solution (2.94 mmol) of SWCNTs-MW-3Cl at −75 °C.

two stages over which the conductivity decreases. First, there is an exponential decay unlike either the exothermic reaction associated with air exposure or the zero order reaction observed with significant catalyst residue. The decay does not follow simple (first- or second-order) kinetics, and thus presumably involves multiple reaction steps. This is followed after ca. 80 min by a period of exceptionally slow zero-order decay (k = 0.08 s^{-1}), and finally after ca. 250 min a final period of stability. Given each of these reactions are significantly slower than any

Table 3. Atomic composition (%) of SWCNTs as determined from XPS

sample	C 1s (%)	O 1s (%)	Fe 2p (%)	Li 1s (%)	Cl 2p (%)
raw SWCNTs	95.0	3.5	1.5		
SWCNT-3Cl	93.5	4.4			2.1
C_{12}–SWCNT-MW-3Cl	96.4	3.4		0.1	

DOI: 10.1021/acsami.7b12857
ACS Appl. Mater. Interfaces XXXX, XXX, XXX–XXX

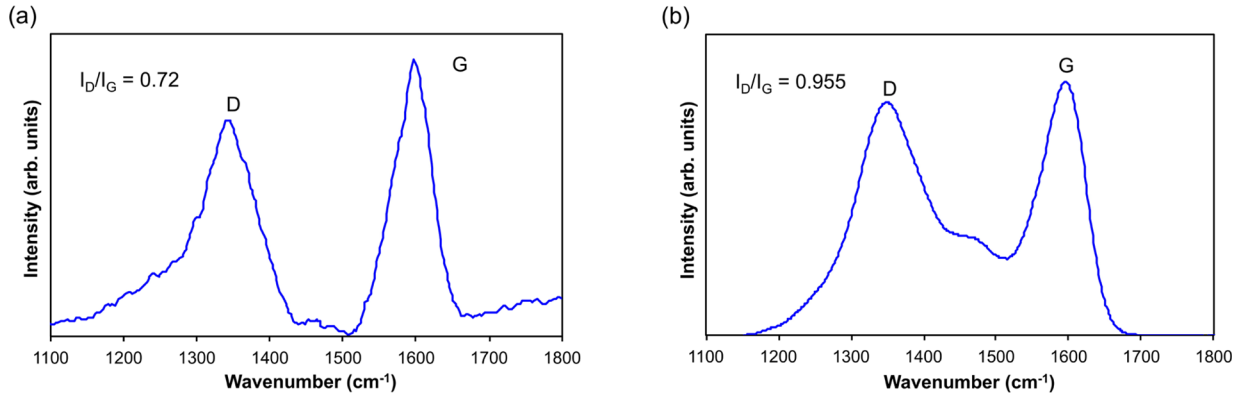

Figure 9. Raman spectra of C_{12}−SWCNTs formed from the reaction of SWCNT-MW-3Cl with Li/NH_3 and 1-iodododecane at −75 °C with (a) Li:C = 3:1 and (b) Li:C = 6:1.

of the quenching reactions, we propose that these are associated with the formation of the reduced SWCNTs.

Given that the chlorine purification occurs via the reaction of Fe/Fe_3O_4/Fe_2O_3 with Cl_2,[18,21,22] and the microwave reaction "exposes" a high proportion of the catalyst residue,[22] any remaining material will be significantly encapsulated. It is reasonable to assume, therefore, that the rate of electron transfer between this deeply encapsulated catalyst residue and the $Li^+[e^-(NH_3)_n]$ solvate will be slower "through" the carbon encapsulate. As would be expected, functionalization of the SWCNT-MW-3Cl with 1-iodododecane results in the formation of C_{12}−SWCNTs with the highest I_D/I_G ratio (0.72) achieved thus far before the effect of catalyst residue was accounted for (Figure 9a).[14] XPS analysis of the C_{12}−SWCNTs shows no chlorine, but traces of trace of residual Li (Table 3)

Controlling the Quantity of Lithium. Using SWCNT-MW-3Cl with <5% Fe, a modified Birch reduction was examined in order to determine the minimum Li:C ratio. Based on literature,[6,13] previous attempts at functionalization involved large ratios of Li:C, sometimes exceeding 20:1. These ratios are unsuitable for scalability due to projected cost issues and lithium waste produced. It was hoped that a Li:C = 1:1 should be sufficient to provide excess electrons for the Birch reduction with a single-electron transfer mechanism. A minimal amount of lithium is ideal because higher lithium ratios provide reactant for competing side reactions, adding undesired product. However, the competing effect of lithium amide formation is unknown, causing the functionalization procedure to require the usage of a higher Li:C ratio.

Tests were performed with decreasing molar Li:C ratio to determine the optimal stoichiometry for stable conductivity, and the highest functionalization. The ∼5% Fe SWCNT-MW-3Cl began to exhibit stable conductivity in Li-NH_3 solution with a Li:C ratio = 6:1, which also results in a I_D/I_G ratio close to the desired 1:1 value (Figure 9b) which comes close to published literature reports (Figure 10) that used higher C:Li ratios of 1:20.[13] Although the quantity of free electrons does not directly affect the reaction, varying amounts of NH_3 displays fluctuating conductivity trends due to more volume for competing side reactions.

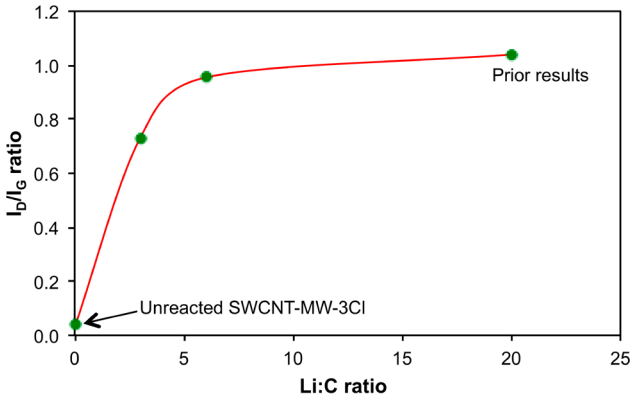

Figure 10. Plot of I_D/I_G ratio obtained from the Raman spectra of the product from the reaction of SWCNTs with Li/NH_3 and 1-iodododecane as a function of Li:C molar ratio in comparison with previously reported values.[6,13]

CONCLUSIONS

We have demonstrated a simple, low cost and scalable means of reproducible Birch reduction-based functionalization of SWCNTs using an in-house built dual reactor apparatus. The effect of catalyst residue was tested and found to have a drastic effect on the extent of functionalization as quantified by Raman spectroscopy of the functionalized SWCNTs. The catalyst residue was found to catalytically quench the formation of stable reduced SWCNT species required for the reaction with alkyl iodides (RI). A combined chlorination-microwave purification process was used to remove excess iron catalyst, and allowed for a lower Li:C ratio to be employed while achieving a high I_D/I_G for R-SWCNT. This new understanding of the factors influencing the functionalization chemistry will help reduce material and process cost, and also increase the selectivity of the reaction toward the desired product with a 1:1 I_D/I_G.

ASSOCIATED CONTENT

Supporting Information

The Supporting Information is available free of charge on the ACS Publications website at DOI: 10.1021/acsami.7b12857.

XPS and Raman spectra of the product from the reaction of SWCNT-Cl_n with Li/NH_3 and 1-iodododecane at −35 °C. TGA of SWCNT-*n*l (PDF)

AUTHOR INFORMATION

Corresponding Authors

*(A.R.B.) E-mail: arb@rice.edu or a.r.barron@swansea.ac.uk.
*(W.W.A.) E-mail: w.adams@rice.edu.

DOI: 10.1021/acsami.7b12857
ACS Appl. Mater. Interfaces XXXX, XXX, XXX−XXX

ORCID

W. Edward Billups: 0000-0002-9411-8864

Andrew R. Barron[β]: 0000-0002-2018-8288

Author Contributions

The manuscript was written through contributions of all authors. All authors have given approval to the final version of the manuscript.

Notes

The authors declare no competing financial interest.

■ ACKNOWLEDGMENTS

Financial support was provided by the Office of Naval Research (N00014-15-2717), the Welsh Government Sêr Cymru National Research Network in Advanced Engineering and Materials (NRN-150), the Robert A. Welch Foundation (C-0002), and Lockheed Martin Corporation. The project was supported by generous donations from Judy Ley Allen, Stan and Reinnette Marek, and Robert Shaddox and Julie Pryzant. We acknowledge the contribution of Dr. Bruce Weisman in the early stages of this work and for his input in all Group meetings discussing the research and the manuscript. Dr. Robert H. Hauge died 17 March 2016.

■ REFERENCES

(1) Hirsch, A. Functionalization of Single-Walled Carbon Nanotubes. *Angew. Chem., Int. Ed.* **2002**, *41*, 1853−1859.

(2) Sun, Y.-P.; Fu, K.; Lin, Y.; Huang, W. Functionalized Carbon Nanotubes: Properties and Applications. *Acc. Chem. Res.* **2002**, *35*, 1096−1104.

(3) Georgakilas, V.; Kordatos, K.; Prato, M.; Guldi, D. M.; Holzinger, M.; Hirsch, A. Organic Functionalization of Carbon Nanotubes. *J. Am. Chem. Soc.* **2002**, *124*, 760−761.

(4) Mittal, G.; Dhand, V.; Rhee, K. Y.; Park, S.-J.; Lee, W. R. A Review on Carbon Nanotubes And Graphene as Fillers in Reinforced Polymer Nanocomposites. *J. Ind. Eng. Chem.* **2015**, *21*, 11−25.

(5) Parveen, S.; Rana, S.; Fangueiro, R. A Review on Nanomaterial Dispersion, Microstructure, and Mechanical Properties of Carbon Nanotube and Nanofiber Reinforced Cementitious Composites. *J. Nanomater.* **2013**, *2013*, 710175.

(6) Liang, F.; Sadana, A. K.; Peera, A.; Chattopadhyay, J.; Gu, Z.; Hauge, R. H.; Billups, W. E. A Convenient Route to Functionalized Carbon Nanotubes. *Nano Lett.* **2004**, *4*, 1257−1260.

(7) Chattopadhyay, J.; Sadana, A. K.; Liang, F.; Beach, J. M.; Xiao, Y.; Hauge, R. H.; Billups, W. E. Carbon nanotube salts. Arylation of Single-Wall Carbon Nanotubes. *Org. Lett.* **2005**, *7*, 4067−4069.

(8) Mukherjee, A.; Combs, R.; Chattopadhyay, J.; Abmayr, D. W.; Engel, P. S.; Billups, W. E. Attachment of Nitrogen and Oxygen Centered Radicals to Single-Walled Carbon Nanotube Salts. *Chem. Mater.* **2008**, *20*, 7339−7343.

(9) Anderson, R. E.; Barron, A. R. Solubilization of Single-Wall Carbon Nanotubes in Organic Solvents Without Sidewall Functionalization. *J. Nanosci. Nanotechnol.* **2007**, *7*, 3436−3440.

(10) Ghosh, S.; Wei, F.; Bachilo, S. M.; Hauge, R. H.; Billups, W. E.; Weisman, R. E. Structure-Dependent Thermal Defunctionalization of Single-Walled Carbon Nanotubes. *ACS Nano* **2015**, *9*, 6324−6332.

(11) Chaban, V. V.; Oleg V. Prezhdo, O. V. , Electron Solvation in Liquid Ammonia: Lithium, Sodium, Magnesium, and Calcium as Electron Sources. *J. Phys. Chem. B* **2016**, *120*, 2500−2506.

(12) Gurskii, Z.; Hannongbua, S.; Heinzinger, K. On the Structure of Concentrated Lithium-Liquid Ammonia Solutions. *Mol. Phys.* **1993**, *78*, 461−474.

(13) Liang, F.; Alemany, L. B.; Beach, J. M.; Billups, E. W. Structure Analyses of Dodecylated Single-Walled Carbon Nanotubes. *J. Am. Chem. Soc.* **2005**, *127*, 13941−13948.

(14) Pham, D.; Zhang, K. S.; Lawal, O.; Ghosh, S.; Gangoli, V. S.; Ainscough, T.; Hauge, R. H.; Adams, W. W.; Barron, A. R. Apparatus for Scalable Functionalization of Single-Walled Carbon Nanotubes via the Billups-Birch Reduction. *C* **2017**, *3*, 19.

(15) Fogden, S.; Howard, C. A.; Heenan, R. K.; Skipper, N. T.; Shaffer, M. S. P. Scalable Method for the Reductive Dissolution, Purification, and Separation of Single-Walled Carbon Nanotubes. *ACS Nano* **2012**, *6*, 54−62.

(16) Feng, X.; Irle, S.; Witek, H.; Morokuma, K.; Vidic, R.; Borguet, E. Sensitivity of Ammonia Interaction with Single-Walled Carbon Nanotube Bundles to the Presence of Defect Sites and Functionalities. *J. Am. Chem. Soc.* **2005**, *127*, 10533−10538.

(17) Chiang, I. W.; Brinson, B. E.; Huang, A. Y.; Willis, P. A.; Bronikowski, M. J.; Margrave, J. L.; Smalley, R. E.; Hauge, R. H. Purification and Characterization of Single-Wall Carbon Nanotubes (SWNTs) Obtained from the Gas-Phase Decomposition of CO (HiPco Process). *J. Phys. Chem. B* **2001**, *105*, 8297−8301.

(18) Wright, K. D.; Barron, A. R. Catalyst Residue and Oxygen Species Inhibition of the Formation of Hexahapto-Metal Complexes of Group 6 Metals on Single-Walled Carbon Nanotubes. *C* **2017**, *3*, 17.

(19) Kayat, J.; Gajbhiye, V.; Tekade, R. K.; Jain, N. K. Pulmonary Toxicity of Carbon Nanotubes: a Systematic Report. *Nanomedicine* **2011**, *7*, 40−49.

(20) Kagan, V. E.; Tyurina, Y. Y.; Tyurin, V. A.; Konduru, N. V.; Potapovich, A. I.; Osipo, A. N.; Kisin, E. R.; Schwegler-Berry, D.; Mercer, R.; Castranova, V.; Shvedova, A. A. Direct and Indirect Effects of Single Walled Carbon Nanotubes on RAW 264.7 Macrophages: Role of Iron. *Toxicol. Lett.* **2006**, *165*, 88−100.

(21) Andreoli, E.; Suzuki, R.; Orbaek, A. W.; Bhutani, M. S.; Hauge, R. H.; Adams, W.; Fleming, J. B.; Barron, A. R. Preparation and Evaluation of Polyethyleneimine-Single Walled Carbon Nanotube Conjugates as Vectors for Pancreatic Cancer Treatment. *J. Mater. Chem. B* **2014**, *2*, 4740−4747.

(22) Gomez, V.; Irusta, S.; Lawal, O. B.; Adams, W.; Hauge, R. H.; Dunnill, C. W.; Barron, A. R. Enhanced Purification Of Carbon Nanotubes by Microwave and Chlorine Cleaning Procedures. *RSC Adv.* **2016**, *6*, 11895−11902.

(23) Zhang, L.; Zhang, J.; Schmandt, N.; Cratty, J.; Khabashesku, V. N.; Kelly, K. F.; Barron, A. R. AFM and STM Characterization of Thiol and Thiophene Functionalized SWNTs: Pitfalls in the Use of Chemical Markers to Determine the Extent of Side-Wall Functionalization in SWNTs. *Chem. Commun.* **2005**, 5429−5430.

(24) Greenfield, A.; Schindewolf, U. Kinetics of the Birch Reduction. *Ber. Bunsenges. Phys. Chem.* **1998**, *102*, 1808−1814.

(25) Xu, H.; Li, M.; Wang, H.; Miao, J.; Zou, L. Fenton Reagent Oxidation and Decolorizing Reaction Kinetics of Reactive Red SBE. *Energy Procedia* **2012**, *16*, 58−64.

(26) Cui, K.; Yi, H.; Zhou, Z.-J.; Zhuo, Q.-F.; Bing, Y.-X.; Guo, W.-W.; Xu, Z.-C. Fenton Oxidation Kinetics and Intermediates of Nonylphenol Ethoxylates. *Environ. Eng. Sci.* **2014**, *31*, 217−224.

(27) Hashemian, S. Fenton-Like Oxidation Of Malachite Green Solutions: Kinetic And Thermodynamic Study. *J. Chem.* **2013**, *2013*, 809318.

(28) Vitale, A. A.; Bernatene, E. A.; Vitale, M. G.; Pomilio, A. B. New Insights of the Fenton Reaction Using Glycerol as the Experimental Model. Effect of O_2, Inhibition by Mg^{2+}, and Oxidation State of Fe. *J. Phys. Chem. A* **2016**, *120*, 5435−5445.

(29) Chattopadhyay, J.; Mukherjee, A.; Hamilton, C. E.; Kang, J. H.; Chakraborty, S.; Guo, W.; Kelly, K. F.; Barron, A. R.; Billups, W. E. Graphite Epoxide. *J. Am. Chem. Soc.* **2008**, *130*, 5414−5415.

(30) Kumar, A.; Reddy, A. L. M.; Mukherjee, A.; Dubey, M.; Zhan, X.; Singh, N.; Ci, L.; Billups, W. E.; Nagurny, J.; Mital, G.; Ajayan, P. M. Direct Synthesis of Lithium-Intercalated Graphene for Electrochemical Energy Storage Application. *ACS Nano* **2011**, *5*, 4345−4349.

(31) Hahne, S.; Schindewolf, U. Temperature and Pressure Dependence of the Nonmetal-Metal Transition in Sodium-Ammonia Solutions (Electrical Conductivity and Pressure-Volume-Temperature Data up to 150 °C and 1000 bar). *J. Phys. Chem.* **1975**, *79*, 2922−2928.

(32) Zimmerman, J. L.; Bradley, R. K.; Huffman, C. B.; Hauge, R. H.; Margrave, J. L. Gas-Phase Purification of Single-Wall Carbon Nanotubes. *Chem. Mater.* **2000**, *12*, 1361−1366.

DOI: 10.1021/acsami.7b12857
ACS Appl. Mater. Interfaces XXXX, XXX, XXX−XXX

(33) Makama, A. B.; Salmiaton, A.; Abdullah, N.; Choong, T. S. Y.; Saion, E. B. Recent Developments in Purification of Single Wall Carbon Nanotubes. *Sep. Sci. Technol.* **2014**, *49*, 2797−2812.
(34) Zhang, Q.; Huang, J.-Q.; Qian, W.-Z.; Zhang, Y.-Y.; Wei, F. The Road for Nanomaterials Industry: A Review of Carbon Nanotube Production, Post-Treatment, and Bulk Applications for Composites and Energy Storage. *Small* **2013**, *9*, 1237−1265.
(35) Karousis, N.; Tagmatarchis, N.; Tasis, D. Current Progress on the Chemical Modification of Carbon Nanotubes. *Chem. Rev.* **2010**, *110*, 5366−5397.
(36) Bucossi, A.; Cress, C. D.; Schauerman, C. M.; Rossi, J. E.; Puchades, I.; Landi, B. J. Enhanced Electrical Conductivity in Extruded Single-Wall Carbon Nanotube Wires from Modified Coagulation Parameters and Mechanical Processing. *ACS Appl. Mater. Interfaces* **2015**, *7*, 27299−27305.
(37) Stobinski, L.; Lesiak, B.; Kövér, L.; Tóth, J.; Biniak, S.; Trykowski, G.; Judek, J. Multiwall Carbon Nanotubes Purification and Oxidation By Nitric Acid Studied by the FTIR and Electron Spectroscopy Methods. *J. Alloys Compd.* **2010**, *501*, 77−84.
(38) Hu, H.; Zhao, B.; Itkis, M. E.; Haddon, R. C. Nitric Acid Purification of Single-Walled Carbon Nanotubes. *J. Phys. Chem. B* **2003**, *107*, 13838−13842.
(39) Rosca, I. D.; Watari, F.; Uo, M.; Akasaka, T. Oxidation of Multiwalled Carbon Nanotubes by Nitric Acid. *Carbon* **2005**, *43*, 3124−3131.
(40) Ogrin, D.; Chattopadhyay, J.; Sadana, A. K.; Billups, E. W.; Barron, A. R. Epoxidation and Deepoxidation of Single-Walled Carbon Nanotubes: Quantification of Epoxide Defects. *J. Am. Chem. Soc.* **2006**, *128*, 11322−11323.
(41) Pełech, I.; Pełech, R.; Narkiewicz, U.; Moszyński, D.; Jędrzejewska, A.; Witkowski, B. Chlorination of Carbon Nanotubes Obtained on the Different Metal Catalysts. *J. Nanomater.* **2013**, *2013*, 836281.
(42) Moulder, J. F.; Stickle, W. E.; Sobol, P. E.; Bomben, K. E. *Handbook of X-Ray Photoelectron Spectroscopy*; Eden Prairie (Minnesota): Perkin-Elmer, 1992.
(43) Piao, H.; Adib, K.; Barteau, M. A. A Temperature-Programmed X-ray Photoelectron Spectroscopy (TPXPS) Study of Chlorine Adsorption and Diffusion on Ag(111). *Surf. Sci.* **2004**, *557*, 13−20.
(44) Papirer, E.; Lacroix, R.; Donnet, J.-B.; Nansé, G.; Fioux, P. XPS Study of the Halogenation of Carbon Black-Part 2: Chlorination. *Carbon* **1995**, *33*, 63−72.
(45) Pérez-Cadenas, A. F.; Maldonado-Hódar, F. J.; Moreno-Castilla, C. On the Nature of Surface Acid Sites of Chlorinated Activated Carbons. *Carbon* **2003**, *41*, 473−478.
(46) Vásquez, M.; Cruz, G. J.; Olayo, M. G.; Timoshina, T.; Morales, J.; Olayo, R. Chlorine Dopants in Plasma Synthesized Heteroaromatic Polymers. *Polymer* **2006**, *47*, 7864−7870.
(47) Alemany, L. B.; Zeng, L.; Zhang, L.; Edwards, C. L.; Barron, A. R. Solid State NMR Analysis of Fluorinated Single-Walled Carbon Nanotubes: Assessing the Extent of Fluorination. *Chem. Mater.* **2007**, *19*, 735−744.
(48) Fruehan, R. J.; Martonik, L. J. The Rate of Chlorination of Metals and Oxides: Part III. The Rate of Chlorination of Fe_2O_3 and NiO in Cl_2 and HCl. *Metall. Trans. A* **1973**, *4*, 2793−2797.

DOI: 10.1021/acsami.7b12857
ACS Appl. Mater. Interfaces XXXX, XXX, XXX−XXX